

EXPERIMENTAL RESEARCH ON YSZ TBC STRUCTURE DEBONDING DEFECT DETECTION USING LONG-PULSED EXCITATION OF INFRARED THERMAL WAVE NON-DESTRUCTIVE TESTING

by

**Qingju TANG^{a,b*}, Shuaishuai GAO^a, Yongjie LIU^a,
Yumei LU^a, and Peng XU^a**

^a School of Mechanical Engineering, Heilongjiang University of Science and Technology, Harbin, China

^b School of Electrical Engineering and Automation, Harbin Institute of Technology, Harbin, China

Original scientific paper
<https://doi.org/10.2298/TSCI180513128T>

Thermal barrier coating structure components are prone to coating cracking, debonding and peeling defects in the service process, which affects the work safety and reliability of the hot end parts, even result to catastrophic consequences. Experimental research on Yttria-stabilized zirconia thermal barrier coating structure debonding defect detection has been conducted using long-pulsed excitation of infrared wave non-destructive testing technology. Differences between surface temperature signals of sound and defective regions, detection effect comparison of heating and cooling process, detection effect comparison of different defect preparation methods, and impact of inspection parameters on detection effect were studied and discussed. The research conclusions will provide technical guidance to Yttria-stabilized zirconia thermal barrier coating structure debonding defects using long-pulsed excitation of infrared wave non-destructive testing technology.

Key words: *thermal barrier coating, debonding defects, long-pulsed, infrared wave non-destructive testing technology*

Introduction

Thermal barrier coating (TBC) is one of the best high temperature protective coating, with thermal insulation, corrosion resistance, wear resistance, erosion resistance and other good performance. In recent years, TBC has been widely used in the environment with high temperature and high heat flux, such as power machinery, aviation and space fields [1-3]. Ceramic coatings are generally composed of Yttria stabilized zirconia (YSZ) (6%~8%Y₂O₃ stabilized ZrO₂). Metal buffer layer that is bond coat (BC) is generally composed of MCrAlY, where M is the transition metal Ni, Co or Fe, *etc.*

The TBC structure components are prone to coating cracking, debonding and peeling defects in the service process, which affects the work safety and reliability of the hot end parts, even result to catastrophic consequences. Therefore, it is very necessary to detect and evaluate the state of TBC structure components by using non-destructive testing technology. Infrared thermal wave non-destructive detection technology has many advantages such as high detection efficiency, simple and safe operation, non-contact, *etc.*, provides a new detection tech-

* Corresponding author, e-mail: tangqingju@126.com

nology for the detection of TBC structure components with desbonding defects. At present, it has been widely used in mechanical manufacturing, electric power, construction, chemical and other fields. At present, has been widely used in mechanical manufacturing, electric power, construction, chemical and other fields [4-6].

In this paper, YSZ TBC structure with debonding defects was taken as the research object, and experiments were carried out using long-pulsed excitation of infrared wave non-destructive testing technology. The influence of debonding defects preparation methods, the size of defects, the selection of heating and cooling processes, output power of light source, and sampling frequency on the detection effect was discussed, which could provide some technical guidance for the detection of TBC structure components with debonding defects.

Detection principle

The infrared wave non-destructive testing system with long-pulsed excitation is composed of thermal excitation system, infrared image sequence acquisition system and image sequence processing and analysis system. A light regulating device and function generator was used to generate a pulse signal to halogen lamps, and the heat flux was illuminated on the surface of samples. At the same time, the infrared camera began to capture the temperature variation data of the sample surface, the collected information was stored in the computer, and then processed by the image sequence processing and analysis system.

Experimental study

Sample preparation and experimental methods

The YSZ (6%~8% Y_2O_3 stabilized ZrO_2) was used as the ceramic layer material. Nickel based super alloy GH4169 was selected as the substrate with the size of $140\text{ mm} \times 100\text{ mm} \times 5\text{ mm}$. NiCoCrAlY was used at the interface between the ceramic layer and super alloy. The TBC was prepared by plasma spray method. At present, blind flat-bottomed holes are generally used to simulate debonding defects, and here is called as Method 1. The simulation debonding defects in specimen was prepared by electric discharge machining technology. In this paper, blind circular flat bottomed holes were machined in the super alloy substrate, and the depth was to the bottom surface of ceramic layer. Then the holes were filled with super alloy round bars, and quartz powder was set at the interface between the bottom surface of ceramic layer and super alloy round bars, which were simulated as air debonding defects. Here the defects preparation method is called as Method 2.

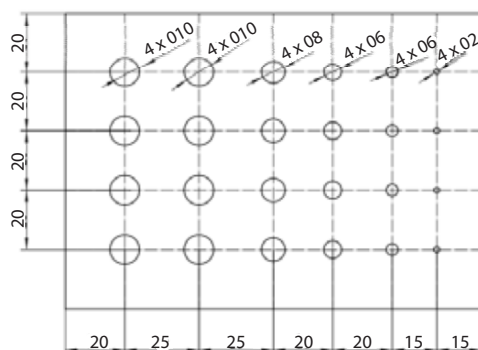


Figure 1. Size of defects

Figure 1 shows the YSZ TBC structure specimen with debonding defects. Blind bottomed hole defects of the first low were not filled with super alloy round bars and quartz powder, which were used for detection effect comparison of Methods 1 and 2.

At room temperature, the standard atmospheric pressure and natural-convection conditions, inspection experiments have been carried out by setting different output power of light source and sampling frequency. Differences between surface temperature signals of sound and defective regions, detection effect comparison of heating and cooling process, detection effect

comparison of different defect preparation methods, and impact of inspection parameters on detection effect were studied.

Differences between surface temperature signals of sound and defective regions

In order to make the thermal image data collected in the tests under the same number grade, normalization was conducted [7, 8]:

$$p_n = \frac{p - p_{\min}}{p_{\max} - p_{\min}} \tag{1}$$

where p is raw data, p_n – the sample data after normalization, p_{\max} , and p_{\min} means the maximum and minimum value of p .

Figure 2 shows an original thermal image collected in the experiments under inspection parameters of output power of light source 2000 W, sampling frequency 30 Hz, sampling time 20 seconds, and pulse duration 15 seconds. From fig. 2, it can be seen that the defects shew very vague, surface temperature difference was overwhelmed by a large number of irrelevant noise, and it is very difficult to identify defects from original thermal images.

The specimens cannot be in a state of absolute thermal equilibrium before actual detection, due to the existence of various noises. In order to reduce the effect of interference on the experimental results, first a background thermal image was captured before halogen lamp excitation, as shown in fig. 3. Then set corresponding inspection parameters, capture original infrared thermography sequence, and make subtraction operation the background thermal image, as shown in fig. 4, which can reduce the influence of background noise, and improve the contrast between defective and sound regions significantly.

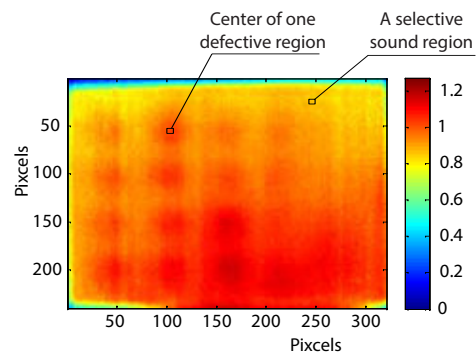


Figure 2. An original thermal image collected in the experiments

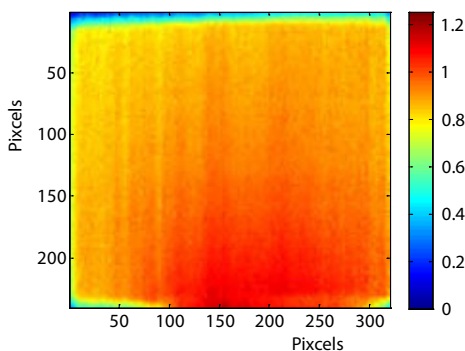


Figure 3. A background thermal image

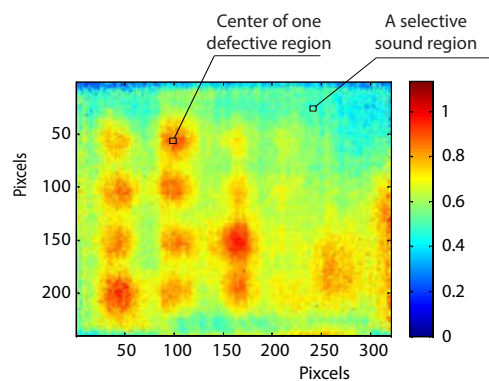


Figure 4. After subtraction operation

Figure 5 shows the surface temperature difference variation of defective and sound regions. It can be seen that the surface temperature difference of defective regions is more obvious than that of the sound regions.

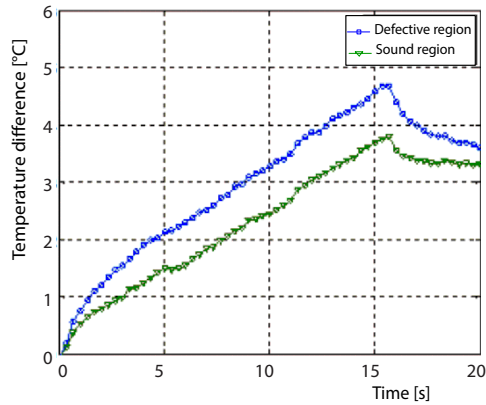


Figure 5. The surface temperature difference variation of defective and sound region

From fig. 4, it can be seen that even if after subtracting background thermal image, serious noise interference still exists, and the defects shows relatively vague. In order to further improve the contrast between defective and sound areas, Fourier transform of the image sequence has been done [9-12]. The best amplitude and phase diagrams after Fourier transform were shown as fig. 6, which the amplitude diagram eliminates a lot of noise, and increased the contrast significantly.

In order to analyzed the relationship between the amplitude signal and defect characteristics, the amplitude contrast was calculated using:

$$K = \frac{[F_{Di} - F_N]}{F_N} \quad (2)$$

where F_{Di} is the amplitude of the defect center, $i = 1 \sim 24$, F_N means the amplitude of the sound regions.

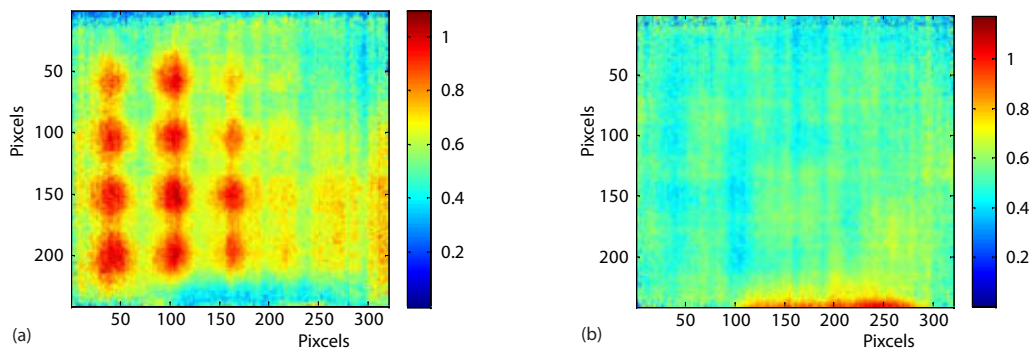


Figure 6. The beat amplitude and phase diagram after Fourier transform; (a) the best amplitude diagram, (b) the best phase diagram

Detection effect comparison of heating and cooling process

Set the output power of light source $P = 2000$ W, sampling frequency $f = 60$ Hz, sampling time $t = 30$ s, and heating pulse duration $W = 15$ s. In the heating process (0~15 s), surface temperature distribution of different moment is shown in fig. 7. At the beginning stage, the surface temperature field is uneven, and the temperature difference between defective and sound regions is not obvious; In the medium heating process, the overall surface temperature distribution began to uniform slowly, and the temperature difference between defective and sound regions got more and more obvious. The uneven heating of the right edge is mainly due to the uneven thickness distribution of the coating resulting to uneven emissivity of the specimen surface. After turning off the halogen lamp, the surface temperature of the specimen gradually tends to thermal equilibrium, and temperature difference gradually decreases, which result

to the gradual decreasing of image contrast and vague conour of defects. In the cooling process (15~30 s), surface temperature distribution of different moment is shown in fig. 8.

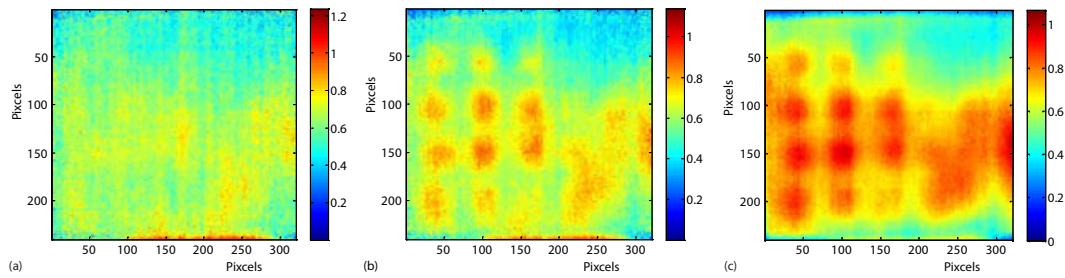


Figure 7. Surface temperature distribution of different moment in the heating process; (a) 0.5 s, (b) 2 s, and (c) 10 s

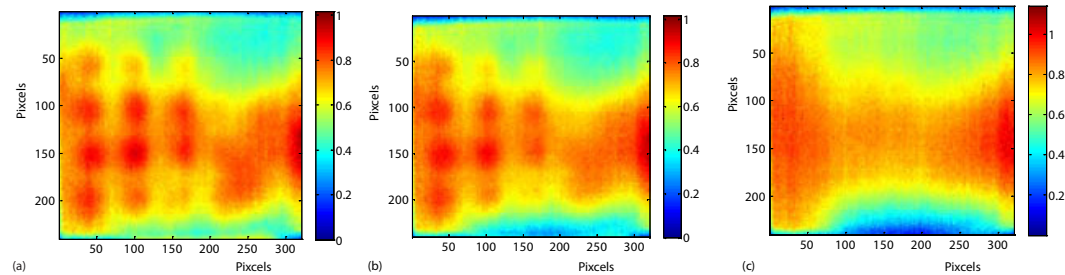


Figure 8. Surface temperature distribution of different moment in the cooling process; (a) 16 s, (b) 20 s, and (c) 26 s

Fourier transform has been done to the image sequence of heating and cooling process, respectively, and the optimal amplitude diagram was shown in fig. 9. The left 3 rows of defects displayed relatively clear, while the fourth row fuzzy, and the 5th and 6th row hardly can be seen. The maximum amplitude display effect differences of heating and cooling process were very small, so either the image sequence arrived from heating process or that of cooling process can be selected to process.

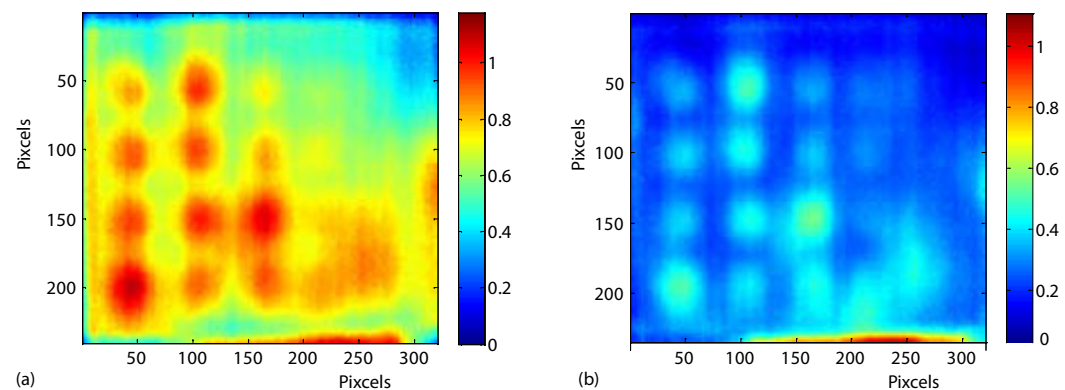


Figure 9. Comparison of the optimal amplitude of heating and cooling processes; (a) heating process, (b) cooling process

Detection effect comparison of different defect preparation methods

From the theoretical point of view, there are differences between blind bottomed holes and real debonding defects, which will change the transfer direction of thermal waves. Two row defects of diameter 10 mm were prepared using Methods 1 and 2. Set the output power of light source 2000 W, sampling frequency 60 Hz, and sampling time 20 seconds. Figure 10 shows the optimal amplitude diagram, from which it can be seen the amplitude difference between defective and sound regions of Method 2 is higher than that of Method 1. Figure 11 shows the surface temperature difference variation of Method 1 and 2. The peak value of Method 2 is higher than that of Method 1, which is conducive to defect detection. Method 2 proposed in this paper provides a new method for the preparation of coating structure debonding defects.

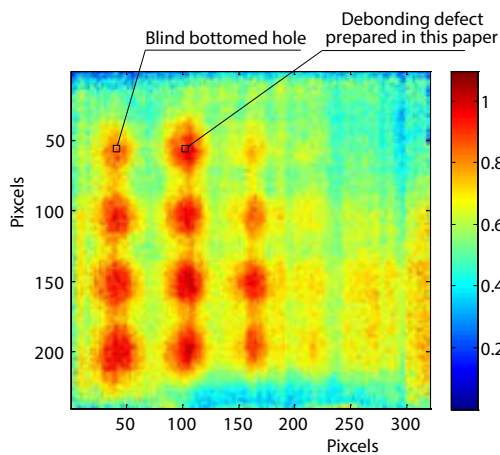


Figure 10. Optimal amplitude diagram

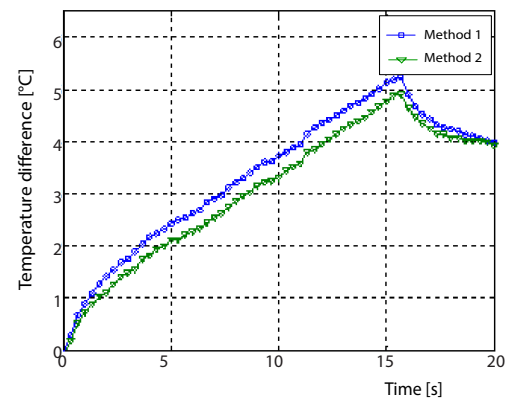


Figure 11. Surface temperature difference variation of Methods 1 and 2

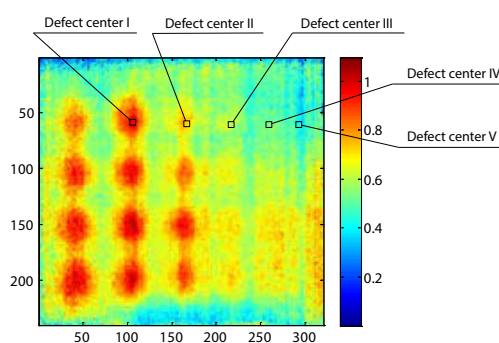


Figure 12. Optimal amplitude diagram

Influence of defect diameter

Set the output power of light source 2000 W, sampling frequency 60 Hz, sampling time 20 seconds, and pulse duration 15 seconds. Figure 12 shows the optimal amplitude diagram, the central regions of defects with different diameter were marked. Figure 13 shows the relationship between amplitude contrast and defect diameter. Larger defect diameter corresponds to larger amplitude contrast, which means more obvious difference between defective and sound regions, and more advantageous to the defect detection.

Influence of the output power of the light source

Set the sampling frequency 60 Hz, sampling time 20 seconds, and pulse duration 15 seconds, the output power of light source 1000 W, 1200 W, 1600 W, and 2000 W, respectively.

The optimum amplitude diagram got from each experiment was shown in fig. 14. The image was very blurred when the output power of light source is set as 1000 W. Defects became clear gradually with the increase of the output power of light source. Three rows of large diameter defects have been displayed gradually clear, when the output power of light source was set as 1600 W. Defects with the diameter of 10 mm and 8 mm can be relatively clear displayed, when the output power of light source was set as 2000 W.

Amplitudes of the marked defective and sound regions under different output power were calculated, and the relationship between thermal amplitude contrast and the output power of light source were arrived, as shown in fig. 15. From fig. 15, it can be seen that the amplitude contrast increases with the increase of the output power of the light source. It means that the stronger the output power of light source, the better detection results can be arrived.

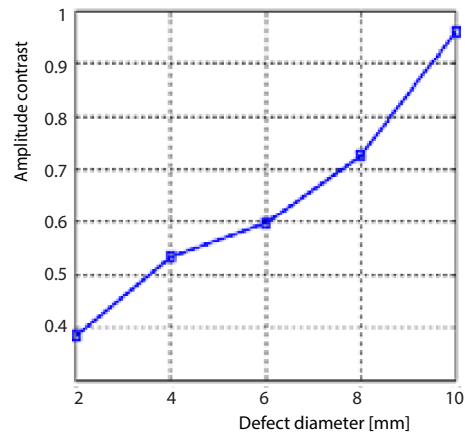


Figure 13. The relationship between amplitude contrast and defect diameter

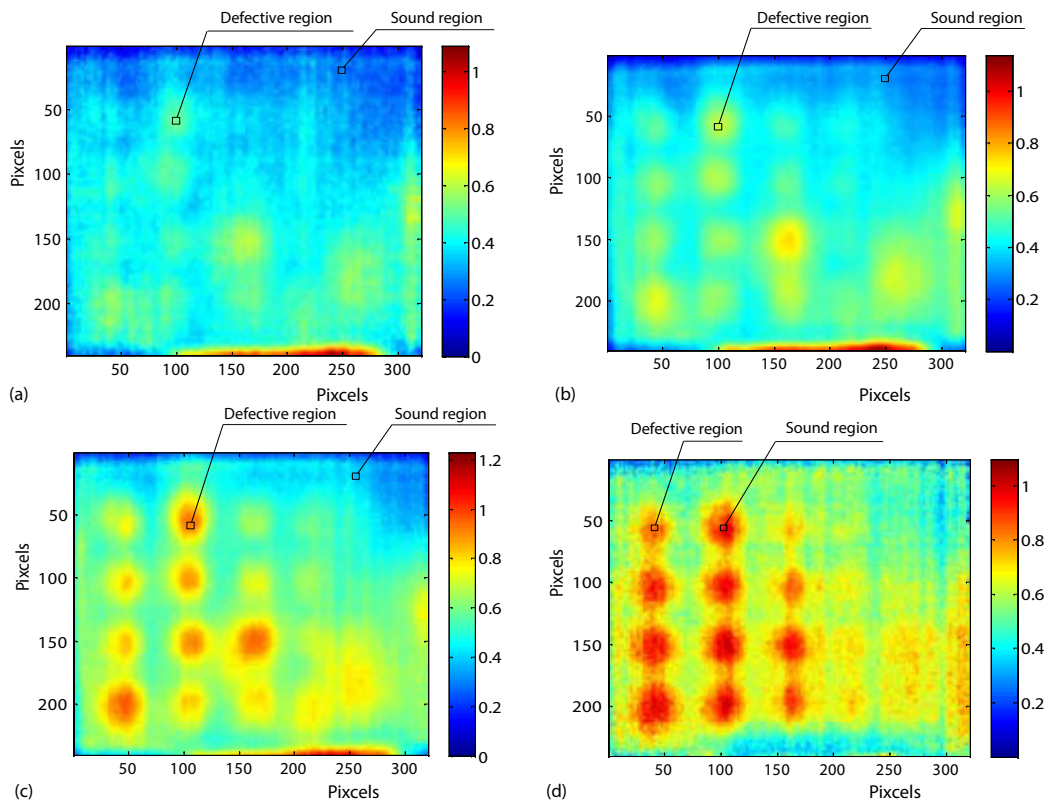


Figure 14. Influence of the output power of the light source; (a) 1000 W, (b) 1200 W, (c) 1600 W, and (d) 2000 W

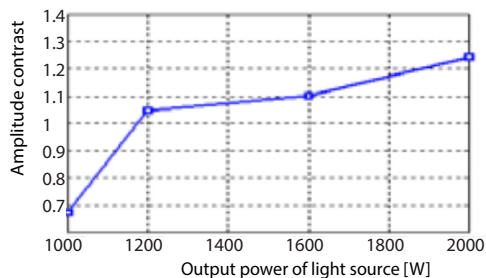


Figure 15. The relationship between amplitude contrast and the output power of light source

Conclusions

Experimental research on YSZ thermal barrier coating structure debonding defect detection has been conducted using long-pulsed excitation of infrared wave non-destructive testing technology. Differences between surface temperature signals of sound and defective regions, detection effect comparison of heating and cooling process, detection effect comparison of different defect preparation methods, and impact of inspection parameters on detection effect were studied and discussed. Results show as follows.

- The image sequence after subtraction treatment by background image was processed using Fourier transform algorithm, and amplitude and phase diagrams were arrived, in which amplitude diagram eliminated a lot of noise, and improve the contrast significantly.
- The maximum amplitude display effect differences of heating and cooling process were very small, so either the image sequence arrived from heating process or that of cooling process can be selected to process.
- Compared to conventional debonding defects preparation method, the method proposed in this paper is more close to the actual defects, and can arrive relatively higher peak value than that of conventional method. It provides a new method for the preparation of coating structure debonding defects.
- Larger defect diameter corresponds to larger amplitude contrast, which means more obvious difference between defective and sound regions, and more advantageous to the defect detectio.
- The amplitude contrast increases with the increase of the output power of the light source, and the better detection results can be arrived The above research conclusions will provide technical guidance to YSZ thermal barrier coating structure debonding defects using long-pulsed excitation of infrared wave non-destructive testing technology.

Acknowledgment

This study is sponsored by National Natural Science Foundation of China (No. 51775175), Special Financial Grant from the China Postdoctoral Science Foundation (No. 2016T90278), China Postdoctoral Science Foundation the Fifty-Eighth Batch (no. 2015M80258), and Heilongjiang Postdoctoral Science Foundation (No. LBH-Z15091).

Nomenclature

F_{Di} – amplitude of the defect center	p_{\max} – maximum value of p , [K]
F_N – amplitude of the sound regions, [K]	p_{\min} – minimum value of p , [K]
K – amplitude contrast	p_n – sample data after normalization
p – raw temperature data, [K]	

References

- [1] Yang, G., et al., Infrared Radiative Properties of EB-PVD Thermal Barrier Coatings, *International Journal of Heat and Mass Transfer*, 94 (2016),4, pp. 199-210
- [2] Loghman-Estarki, M. R., et al., Evaluation of Hot Corrosion Behavior of Plasma Sprayed Scandia and Yttria Co-Stabilized Nanostructured Thermal Barrier Coatings in the Presence of Molten Sulfate and Vanadate Salt, *Journal of the European Ceramic Society*, 35 (2015), 2, pp. 693-702

- [3] Rodriguez, F. L., *et al.*, Inverse Heat Transfer Approach for IR Image Reconstruction: Application Thermal Non-Destructive Evaluation, *Applied Thermal Engineering*, 33-34 (2012), 1, pp. 109-118
- [4] Dudzik, S., Two-Stage Neural Algorithm for Defect Detection and Characterization Uses an Active Thermography, *Infrared Physics & Technology*, 71 (2015), 7, pp. 187-197
- [5] Lizaranzu, M., *et al.*, Non-Destructive Testing of Composite Materials by Means of Active Thermography-based Tools, *Infrared Physics & Technology*, 71 (2015), 7, pp. 113-120
- [6] Marinetti, S., *et al.*, Thermographic Inspection of TBC Coated Gas Turbine Blades: Discrimination between Coating over-thicknesses and Adhesion Defects, *Infrared Physics and Technology*, 49 (2007), 3, pp. 281-285
- [7] Tabatabaei, N., *et al.*, Thermophotonic Radar Imaging: An Emissivity-Normalized Modality with Advantages over Phase Lock-in Thermography, *Applied Physics Letters*, 98 (2011), 16, pp. 617
- [8] Ibarracastanedo, C., *et al.*, Pulsed Phase Thermography Inversion Procedure Using Normalized Parameters to Account for Defect Size Variations, *Proceedings of SPIE – The International Society for Optical Engineering*, 5782 (2005), Mar., pp. 334-341
- [9] Chang, Y. S., *et al.*, Non-Destructive Testing of CFRP Using Pulsed Thermography and Multi-Dimensional Ensemble Empirical Mode Decomposition, *Journal of the Taiwan Institute of Chemical Engineers*, 61 (2016), Apr., pp. 54-63
- [10] Shin, P. H., *et al.*, Pulsed Phase Thermography Imaging of Fatigue-Loaded Composite Adhesively Bonded Joints, *Ndt and E International*, 79 (2016), Apr., pp. 7-16
- [11] Wang, F., *et al.*, Optical Excitation Fractional Fourier Transform (FrFT) Based Enhanced Thermal-Wave Radar Imaging (TWRI), *Optics Express*, 26 (2018), 17, pp. 21403-21417
- [12] Yang, X., General Fractional Calculus Operators Containing the Generalized Mittag-Leffler Functions Applied to Anomalous Relaxation, *Thermal Science*, 21 (2017), Suppl. 1, pp. S317-S326